that thrive under conditions of limited nutrient availability (*25*, *26*). Specifically, verrucomicrobial abundances were positively correlated with a variety of genes associated with carbohydrate metabolism but were negatively correlated with genes associated with nitrogen metabolism and cell division (Fig. 3D). Verrucomicrobia may thus represent a large component of below-ground communities in regions where changes in the quantity or quality of plant organic matter inputs constrain the growth of more copiotrophic taxa. This hypothesis is congruent with results indicating consistent declines in the relative abundances of Verrucomicrobia when soils from across North America were amended with nutrients (*27*). Likewise, this hypothesis is consistent with recent genomic information obtained from *Spartobacteria aquaticum*, an aquatic Verrucomicrobia that is within the same class as the dominant soil Verrucomicrobia observed here, that appears to specialize on the degradation of more recalcitrant carbon compounds (*28*).

Our reconstructions of microbial diversity and functional capabilities across the tallgrass prairie ecosystem could be used to guide and monitor the hundreds of prairie restoration efforts currently underway throughout the midwestern United States (*29*). Maps of the soil microbial communities that once existed in this ecosystem may provide targets to help improve the long-term success of prairie restoration efforts, as restoration efforts are often more successful when they also try to restore below-ground communities (*30*). Such information may be particularly important if the goal is to restore key ecosystem functions, such as soil carbon sequestration, that are strongly controlled by the below-ground communities. Likewise, deviation in soil microbial communities from the predicted pre-agricultural state could be used to quantify the extent of degradation experienced by soils throughout the native prairie range. More generally, this work demonstrates that we can use recent advances in high-throughput microbial community characterization to reconstruct the biogeographical patterns in the diversity and functional capabilities of microbes across a nearly extinct ecosystem. This approach could be extended more broadly to quantify how historical changes in environmental conditions may have altered the diversity and function of below-ground communities in other systems or to determine how human-induced climate change may alter ecosystem properties in the future.

References and Notes

1. P. Sims, P. Risser, in *North American Terrestrial Vegetation*, M. Barbour, W. Billings, Eds. (Cambridge Univ. Press, New York, 2000), pp. 325–356.
2. F. Samson, F. Knopf, W. Ostlie, *Wildl. Soc. Bull.* **32**, 6–15 (2004).
3. F. Samson, F. Knopf, *Bioscience* **44**, 418–421 (1994).
4. V. J. Allison, Z. Yermakov, R. M. Miller, J. D. Jastrow, R. Matamala, *Soil Biol. Biochem.* **39**, 505–516 (2007).
5. D. R. Huggins *et al.*, *Soil Tillage Res.* **47**, 219–234 (1998).
6. K. Jangid *et al.*, *Soil Biol. Biochem.* **42**, 302–312 (2010).
7. S. G. Baer, D. J. Kitchen, J. M. Blair, C. W. Rice, *Ecol. Appl.* **12**, 1688–1701 (2002).
8. E. J. Martinson *et al.*, *Phys. Geogr.* **32**, 583–602 (2011).
9. S. G. Tringe, E. M. Rubin, *Nat. Rev. Genet.* **6**, 805–814 (2005).
10. N. Fierer *et al.*, *Proc. Natl. Acad. Sci. U.S.A.* **109**, 21390–21395 (2012).
11. N. Fierer, J. Ladau, *Nat. Methods* **9**, 549–551 (2012).
12. N. Fierer *et al.*, *ISME J.* **6**, 1007–1017 (2012).
13. See supplementary materials on *Science* Online.
14. B. A. Hawkins *et al.*, *Ecology* **84**, 3105–3117 (2003).
15. J. A. Gilbert, R. O'Dor, N. King, T. M. Vogel, *Microb. Inform. Exp.* **1**, 5 (2011).
16. H. Hillebrand, B. Matthiessen, *Ecol. Lett.* **12**, 1405–1419 (2009).
17. O. L. Petchey, K. J. Gaston, *Ecol. Lett.* **5**, 402–411 (2002).
18. S. Díaz, M. Cabido, *Trends Ecol. Evol.* **16**, 646–655 (2001).
19. M. Bradford, N. Fierer, in *Soil Ecology and Ecosystem Services*, D. Wall, Ed. (Oxford Univ. Press, Oxford, 2012), pp. 189–198.
20. J. Franklin, J. Miller, *Mapping Species Distributions: Spatial Inference and Prediction* (Cambridge Univ. Press, New York, 2010).
21. J. Ladau *et al.*, *ISME J.* **7**, 1669–1677 (2013).
22. R. K. Colwell, D. C. Lees, *Trends Ecol. Evol.* **15**, 70–76 (2000).
23. G. T. Bergmann *et al.*, *Soil Biol. Biochem.* **43**, 1450–1455 (2011).
24. S. J. Joseph, P. Hugenholtz, P. Sangwan, C. A. Osborne, P. H. Janssen, *Appl. Environ. Microbiol.* **69**, 7210–7215 (2003).
25. U. N. da Rocha, F. D. Andreote, J. L. Azevedo, J. D. van Elsas, L. van Overbeek, *J. Soils Sed.* **10**, 326–339 (2010).
26. P. H. Janssen, P. S. Yates, B. E. Grinton, P. M. Taylor, M. Sait, *Appl. Environ. Microbiol.* **68**, 2391–2396 (2002).
27. K. S. Ramirez, J. M. Craine, N. Fierer, *Glob. Change Biol.* **18**, 1918–1927 (2012).
28. D. P. Herlemann *et al.*, *mBio* **4**, e00569-12 (2013).
29. J. Harris, *Science* **325**, 573–574 (2009).
30. P. Kardol, D. A. Wardle, *Trends Ecol. Evol.* **25**, 670–679 (2010).

Acknowledgments: We thank K. McLauchlan and three anonymous reviewers for their critical feedback on earlier versions of the manuscript; R. Jackson for his help with soil collection and analyses; and J. Henley for her help with the laboratory analyses. Supported by NSF grants DEB-0953331 (N.F.) and DMS-1069303 (K.S.P.), the Howard Hughes Medical Institute (R.K.), Gordon and Betty Moore Foundation grant 3300 (K.S.P.), U.S. Department of Energy contract DE-AC02-06CH11357 (J.A.G.), and USDA National Research Initiative 2005-35101-15335/17371 (R.L.M.). All amplicon data have been deposited in the European Nucleotide Archive under accession number ERP003610; the accession number for the shotgun metagenomic data is ERP003954. Data have also been made available through the Dryad data depository.

Supplementary Materials

www.sciencemag.org/content/342/6158/621/suppl/DC1
Materials and Methods
Figs. S1 to S4
Tables S1 to S4
References (*31*–*50*)

25 July 2013; accepted 2 October 2013
10.1126/science.1243768

Structural Basis for flg22-Induced Activation of the *Arabidopsis* FLS2-BAK1 Immune Complex

Yadong Sun,[1]* Lei Li,[2]* Alberto P. Macho,[3] Zhifu Han,[1]† Zehan Hu,[1] Cyril Zipfel,[3] Jian-Min Zhou,[2]† Jijie Chai[1]†

Flagellin perception in *Arabidopsis* is through recognition of its highly conserved N-terminal epitope (flg22) by flagellin-sensitive 2 (FLS2). Flg22 binding induces FLS2 heteromerization with BRASSINOSTEROID INSENSITIVE 1–associated kinase 1 (BAK1) and their reciprocal activation followed by plant immunity. Here, we report the crystal structure of FLS2 and BAK1 ectodomains complexed with flg22 at 3.06 angstroms. A conserved and a nonconserved site from the inner surface of the FLS2 solenoid recognize the C- and N-terminal segment of flg22, respectively, without oligomerization or conformational changes in the FLS2 ectodomain. Besides directly interacting with FLS2, BAK1 acts as a co-receptor by recognizing the C terminus of the FLS2-bound flg22. Our data reveal the molecular mechanisms underlying FLS2-BAK1 complex recognition of flg22 and provide insight into the immune receptor complex activation.

Innate immunity in higher eukaryotes relies on the perception of conserved signature components of pathogens, termed pathogen-associated molecular patterns (PAMPs), by plasma membrane–localized pattern recognition receptors (PRRs). In plants, PRRs are mainly receptor kinases (RKs) or receptor-like proteins, and several of them carry leucine-rich repeats (LRRs) in their ectodomains for PAMP recognition. Upon recognition of PAMPs, PRRs initiate an array of shared immune responses, leading to PAMP-triggered immunity (*1*).

Present in most higher plant species and critical for antibacterial immunity (*1*), flagellin-sensitive 2 (FLS2) is an LRR-RK and acts as the PRR for bacterial flagellin by recognizing the epitope flg22 (*2*–*6*). Direct recognition of flg22 by FLS2 is sufficient for inducing immune responses, establishing FLS2 as a flagellin receptor (*7*). Flg22 binding nearly instantly triggers FLS2 association with the LRR-RK BRI1-associated kinase 1 (BAK1) (*8*, *9*). BAK1 also interacts with the LRR-RK

[1]School of Life Sciences, Tsinghua University, Beijing 100084, China, and Tsinghua-Peking Center for Life Sciences, Beijing 100084, China. [2]State Key Laboratory of Plant Genomics and National Center for Plant Gene Research, Institute of Genetics and Developmental Biology, Chinese Academy of Sciences, Beijing 100101, China. [3]The Sainsbury Laboratory, Norwich Research Park, Norwich NR4 7UH, UK.

*These authors contributed equally to this work.
†Corresponding author. E-mail: chaijj@mail.tsinghua.edu.cn (J.C.); jmzhou@genetics.ac.cn (J.-m.Z.); hanzhifu@mail.tsinghua.edu.cn (Z.Han)

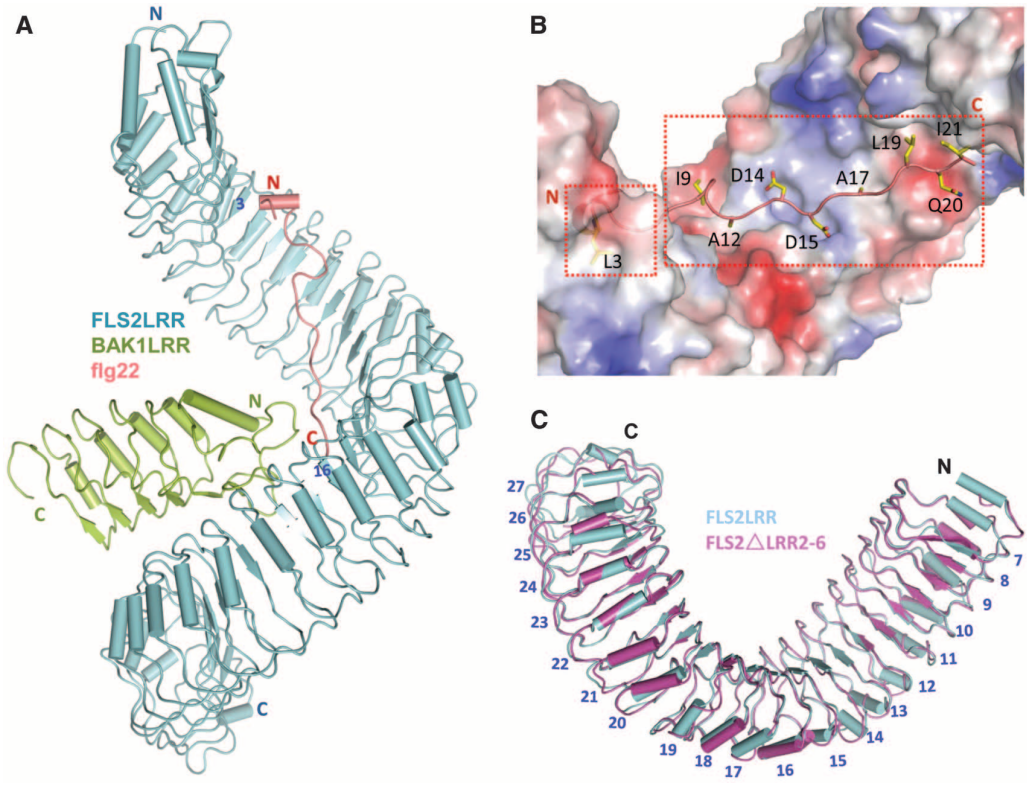

Fig. 1. Ectodomains mediate the flg22-induced heterodimerization of FLS2 and BAK1. (**A**) Overall structure of FLS2LRR-flg22-BAK1LRR. The positions of LRR3 and LRR16 are indicated by blue numbers. "N" and "C" represent the N and C terminus, respectively. Color codes are indicated. (**B**) Flg22 binds to a shallow groove at the inner surface of the FLS2LRR solenoid. FLS2LRR is shown in electrostatic surface (in transparency). The FLS2LRR-interacting residues in flg22 are shown stick. I, Ile; Q, Gln. White, blue, and red indicate neutral, positive, and negative surfaces, respectively. Detailed interactions of the left and right highlighted regions are shown in Fig. 2, A and B, respectively. (**C**) Structural comparison of the ligand-bound FLS2LRR with the free FLS2ΔLRR2-6. For clarity, the N- and C-terminal sides of the flg22-bound FLS2LRR are not shown. Numbers in blue indicate the positions of LRRs.

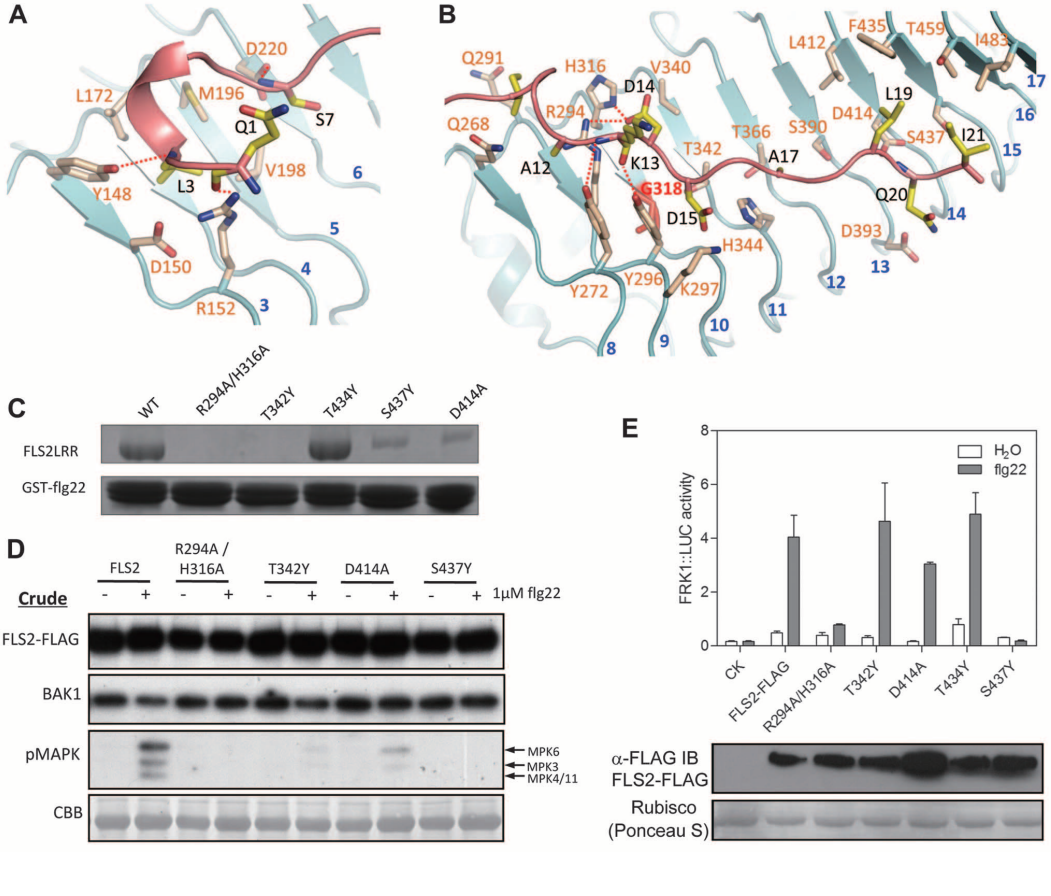

Fig. 2. Mechanism of flg22 recognition by FLS2. (**A**) Interaction of the N-terminal portion (residues 1 to 7) of flg22 with FLS2LRR. The side chains FLS2LRR and flg22 are labeled in cream white and yellow, respectively. (**B**) Interaction of the C-terminal side (residues 8 to 21) of flg22 with FLS2LRR. FLS2 Gly^{318} is indicated in red. K, Lys; S, Ser; T, Thr. (**C**) FLS2LRR mutations reduce interaction with GST-flg22. GST-flg22 bound to GS4B agarose was used to precipitate various FLS2LRR wild-type (WT) and mutant proteins. The bound proteins were visualized by SDS–polyacrylamide gel electrophoresis (PAGE) with Coomassie blue staining. The assay was repeated three times. (**D**) FLS2 mutations compromise MPK phosphorylation. Null *fls2* mutant mesophyll protoplasts were transfected with plasmids as indicated. The samples were separated into two and treated with water (-) or 1 μM flg22 (+). Immunoblots were analyzed by using antibodies against FLAG, BAK1, or pMPK. CBB, Coomassie brilliant blue. (**E**) FLS2 mutations attenuate flg22-induced *FRK1::LUC* expression. Null *fls2* mutant *Arabidopsis* mesophyll protoplasts were transfected with plasmids as indicated along with *35S::R-LUC* and *FRK1::LUC*. The *FRK1::LUC* activity was determined after protoplasts were treated with 1.0 μM flg22 for 10 min. IB, immunoblot.

BR INSENSITIVE 1 (BRI1) to positively regulate brassinosteroid (BR) signaling (*10*, *11*). BAK1 is also called SERK3, a member of the subfamily of SERK LRR-RKs (*12*).

BAK1 also forms heteromers with several other PRRs and is a major component of plant immunity (*13*, *14*). The flg22-induced FLS2-BAK1 heteromerization results in their trans-phosphorylation (*8*, *9*, *15*). Flg22 also induces FLS2- and BAK1-dependent phosphorylation of BIK1 (BOTRYTIS-INDUCED KINASE 1, a receptor-like cytoplasmic kinase) and dissociation of BIK1 from FLS2 for plant immunity (*16*, *17*).

To confirm that the ectodomains of FLS2 and BAK1 are sufficient to form an flg22-induced complex, we used glutathione *S*-transferase (GST) precipitation, gel filtration, and coimmunoprecipitation (Co-IP) to assay their interaction. Collectively, the data from these assays (fig. S1) showed that the extracellular LRR domains of *Arabidopsis* FLS2 (residues 25 to 800, FLS2LRR) and BAK1 (residues 1 to 220, BAK1LRR) formed a monomeric heterodimer induced by flg22. But it remains possible that full-length FLS2 forms homo-oligomers (*18*).

To understand the molecular mechanism underlying FLS2 recognition of flg22, we solved the crystal structure of the FLS2LRR-flg22-BAK1LRR complex at 3.06 Å (Fig. 1A and table S1). None of the dimeric packing related by crystallographic symmetry can be biologically relevant (fig. S2), further supporting the gel filtration data (fig. S1B). This is in contrast with flagellin-induced Toll-like receptor 5 (TLR5) homodimerization (*19*). The structure of FLS2LRR is superhelical (fig. S3) and resembles that of BRI1LRR (*20*, *21*). Flg22, which is well defined by electron density but the last residue (fig. S4), binds to the concave surface of FLS2LRR by running across 14 LRRs (LRR3 to LRR16) (Fig. 1, A and B), confirming previous hypotheses (*22*, *23*). The flg22 binding groove is largely conserved in tomato FLS2 (fig. S5).The FLS2LRR-BAK1LRR heterodimerization is both flg22- and receptor-mediated. The C terminus of flg22 is sandwiched between FLS2LRR and BAK1LRR, whereas direct FLS2LRR-BAK1LRR interactions stem from anchoring of BAK1LRR to the C-terminal portion of FLS2LRR (Fig. 1A). The structural organization of FLS2LRR-BAK1LRR differs from the m-shaped homo- or heterodimeric TLRs (*24*). Nonetheless, the C-termini of BAK1LRR and FLS2LRR are similarly oriented, presumably pointing to the membrane surface.

Interactions of flg22 with FLS2LRR can be divided into two parts separated by a kink (flg22 Asn^{10} and Ser^{11}) in the central region of the peptide (Fig. 1B). Before the kink, the N-terminal seven residues bind to FLS2 LRR2 to LRR6 (FLS2LRR2-6) (Fig. 2A). Thus, deletion of these four LRRs would negate FLS2 interaction with the N- but not the C-terminal segment of flg22, phenocopying an flg22 variant with the N-terminal seven residues deleted (flg15) (*4*). Indeed, an FLS2LRR mutant with five LRRs deleted, FLS2ΔLRR2-6, still formed an flg22-induced complex with BAK1LRR (fig. S6). Structural superposition of the FLS2ΔLRR2-6 mutant with FLS2LRR bound by flg22 and BAK1LRR showed that the two structures are nearly identical (Fig. 1C), with a root mean square deviation = 0.43 Å over 543 Cα-aligned atoms, suggesting that, in the cellular milieu as well, conformational changes in FLS2LRR may not be necessary for flg22 binding and heterodimerization with BAK1LRR.

Both hydrogen bonds and hydrophobic contacts mediate flg22 interaction with FLS2LRR. Flg22 Leu^3 inserts into a hydrophobic pocket of FLS2 (Fig. 2A). In addition to hydrophobic contacts, FLS2 Arg^{152} and FLS2 Tyr^{148} also engage hydrogen bonds with flg22 Gln^1 and flg22 Leu^3, respectively. The two residues are highly varied in tomato FLS2 (fig. S5), which can adversely

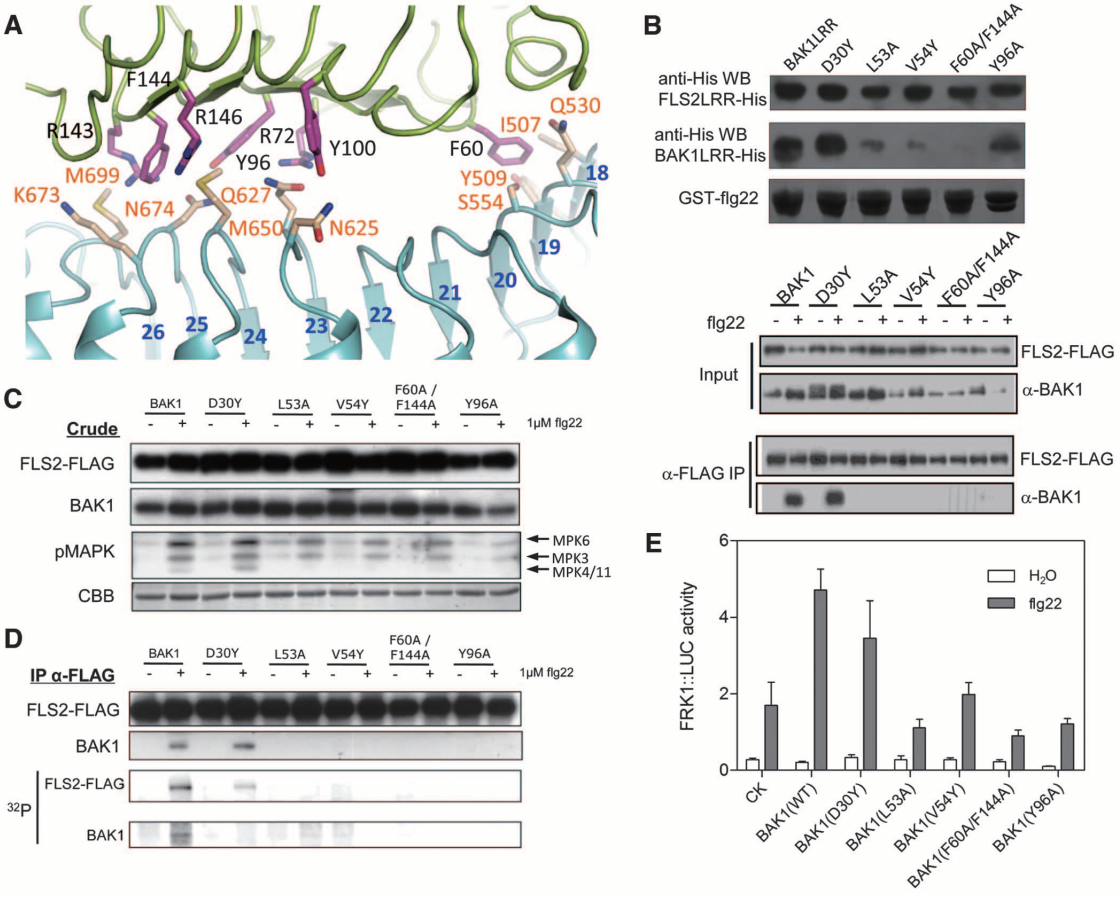

Fig. 3. Direct FLS2LRR-BAK1LRR interactions. (**A**) The C-terminal side of FLS2LRR mediates its interaction with BAK1. M, Met; N, Asn. (**B**) Direct contacts of FLS2 and BAK1 are required for their interaction. (Top) The assays were performed as described in Fig. 2C except that FLS2LRR and BAK1LRR were analyzed by antibodies against His (anti-His). The assay was repeated for three times. (Bottom) Mutagenesis assays for BAK1 mutants in null *bak1-4* mutant mesophyll protoplasts. FLAG- and hemagglutinin (HA)–tagged FLS2 and BAK1 constructs were coexpressed in WT *Arabidopsis* protoplasts. Co-IP assay was performed to detect FLS2-BAK1 interaction after treatment with (+) or without (-) 1.0 μM flg22. (**C**) Mutations of the FLS2-interacting residues in BAK1 compromise MPK phosphorylation. The assays were performed as described in Fig. 2D. (**D**) Mutations of the FLS2-interacting residues in BAK1 compromise FLS2 and BAK1 phosphorylation. Immunoprecipitated FLS2-FLAG was incubated in the presence of radioactive [^{32}P]γ-ATP (adenosine triphosphate). Immunoblots were analyzed by using antibodies against FLAG or BAK1. In vitro phosphorylation is revealed by autoradiography (i.e., ^{32}P). (**E**) FLS2-BAK1 interactions are important for flg22-induced *FRK1* expression. The assays were performed as described in Fig. 2E. Error bars indicate SEM.

affect recognition of the N-terminal part of flg22 by the latter. This may explain the fact that flg15 displays a low activity in *Arabidopsis* but is fully active in tomato cells (*23*). The C-terminal 14 amino acids, particularly those after the kink, form denser interactions with FLS2LRR, burying a surface area of 1817 Å^2 compared with 373 Å^2 by the N-terminal seven amino acids. Consistently, flg15 still bound FLS2LRR (fig. S7A), agreeing with previous cell-based assays (*3*). Flg22 Asp^{14} and Asp^{15}, important for FLS2 interacting (fig. S7A) and immunogenic activities (*3*), bind to two positively charged pockets (Figs. 1B and 2B). The hydrogen bonds formed between FLS2 Tyr^{272} and Tyr^{296} and flg22 Lys^{13} also contribute to the interactions around this interface. In contrast, flg22 Asn^{10} and flg22 Lys^{13} (whose side chain is not involved in interaction with FLS2LRR) are solvent-exposed (fig. S4), and their mutations generated little effect on the flg22 activity (*3*). Flg22 Leu^{19} and Ile^{21} bind to two neighboring hydrophobic pockets. Mutation of flg22 Ala^{17} that contacts FLS2 Thr^{366} underneath to tyrosine (Fig. 2B) reduced flg22 interaction with FLS2LRR (fig. S7A). All the amino acids critical for flg22 binding to FLS2LRR are conserved among FLS2-activating bacteria (fig. S8).

Further supporting our structural observations, a precipitation assay showed that FLS2 with two mutations, Arg^{294} and His^{316} to Ala (*24*), R294A/H316A, resulted in no FLS2LRR-flg22 interaction (Fig. 2C), phenocopying flg22 D14A (D, Asp) (*3*). FLS2 Thr^{342} is located immediately underneath the peptide (Fig. 2B). Mutation of this residue, but not the unrelated FLS2 Thr^{434}, to the bulkier tyrosine abolished the interaction with GST-flg22. Consistently, FLS2 G318R (G, Gly) (Fig. 2B) caused by ethyl methanesulfonate–induced mutation *fls2-24* does not bind flg22 (*4*). Mutations of other FLS2 residues from the interface also compromised interaction with GST-flg22 (Fig. 2C). The mutations affecting FLS2LRR recognition of flg22 disrupted flg22-induced FLS2-BAK1 interaction in *Arabidopsis* protoplasts (fig. S9). Furthermore, flg22-induced FLS2 and BAK1 phosphorylation (fig. S9), mitogen-activated protein kinase (MPK) activation (Fig. 2D) and expression of *FRK1::LUC* (Fig. 2E), a reporter gene induced by multiple PAMPs, were also attenuated when the FLS2 mutants were transiently expressed in null *fls2* mesophyll protoplasts. Together, these results indicate that these residues are functionally important in the plant cell.

A cluster of bulky BAK1 amino acids, including Arg^{72}, Tyr^{96}, Tyr^{100}, Arg^{143}, Phe^{144}, and Arg^{146}, directly contacts with those from FLS2LRR23-26 (Fig. 3A), whereas BAK1Phe^{60} interacts with residues from FLS2LRR18-20. These FLS2-interacting residues are conserved between *Arabidopsis* BAK1 and tomato SERK3 (fig. S10). Supporting the structural observations, BAK1 F60A/F144A (F, Phe) and BAK1 Y96A (Y, Tyr), but not the negative control BAK 1D30Y, attenuated flg22-induced FLS2-BAK1 heterodimerization in the precipitation assay and in null mutant *bak1-4* mesophyll protoplasts (Fig. 3B). These critical BAK1 amino acids were also important for flg22-induced FLS2 and BAK1 phosphorylation (Fig. 3, C and D).The activation of MPKs by flg22 seems differently affected by the BAK1 mutations, because the activation of MPK3 and MPK6 was slightly diminished 10 min after treatment with the peptide, whereas MPK4/MPK11 was not activated to a detectable level at the same time point (Fig. 3C). Moreover, unlike wild-type BAK1, these critical BAK1 mutants (Fig. 3E) only partially restored the expression of *FRK1::LUC* to null mutant *bak1-4* mesophyll protoplasts. Consistently, the BAK1 L53A, V54Y, and Y96A (L, Leu; V, Val) transgenic lines were abolished or severely compromised in production of reactive oxygen species (fig. S11).

The C-terminal segment of flg22 bridges FLS2LRR and BAK1LRR (Fig. 1A), reminiscent of auxin that act as a molecular "glue" to connect its receptor with a signaling partner (*25*). Flg22 Gly^{18}, conserved among the FLS2-activating bacterial flagellins but not in non–FLS2-eliciting bacteria (fig. S8), fits in the inner-curved loop (residues 52 to 54) of BAK1 but makes no contact with FLS2LRR (Fig. 4A). Flg22-BAK1LRR

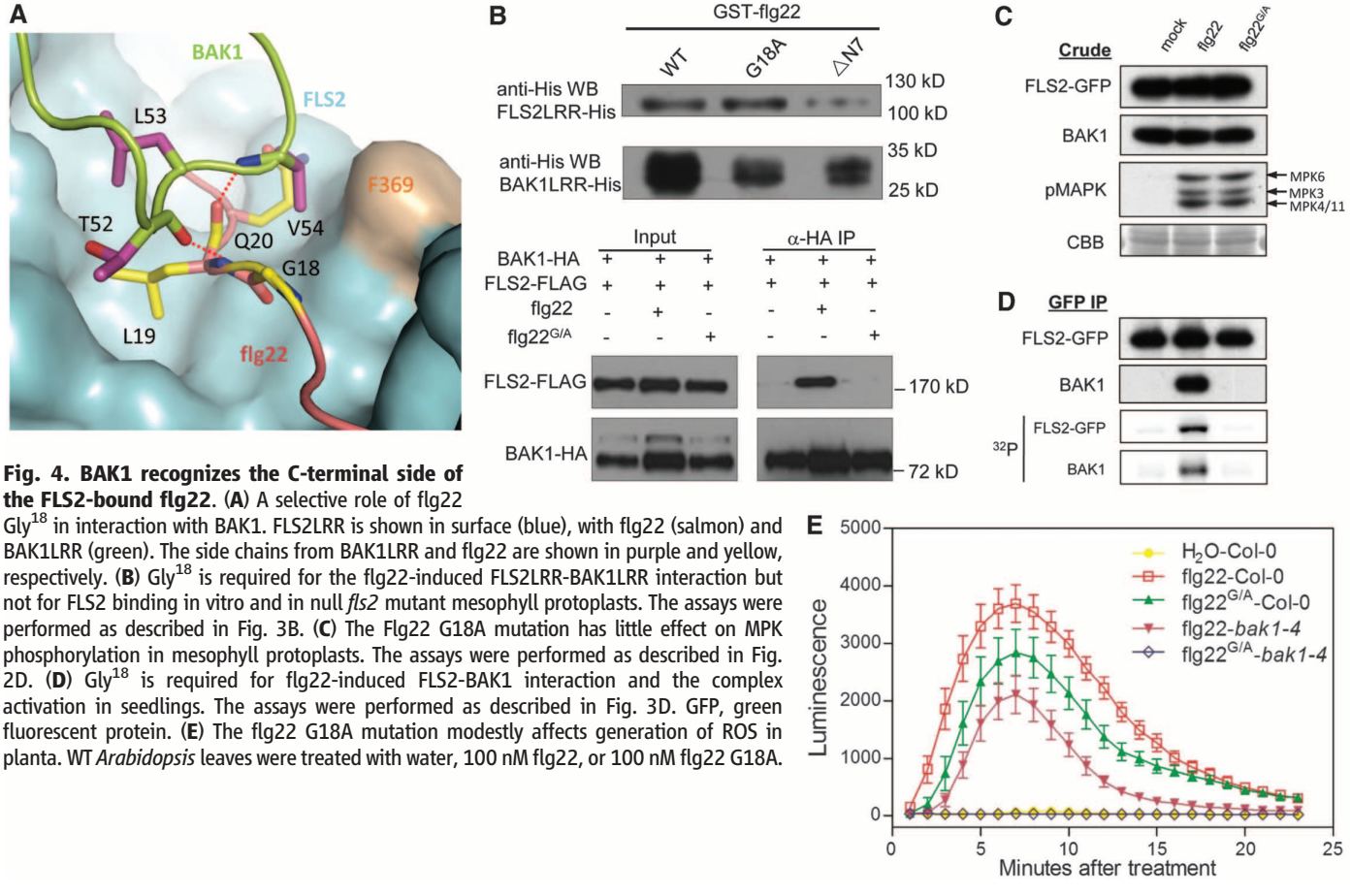

Fig. 4. BAK1 recognizes the C-terminal side of the FLS2-bound flg22. (**A**) A selective role of flg22 Gly^{18} in interaction with BAK1. FLS2LRR is shown in surface (blue), with flg22 (salmon) and BAK1LRR (green). The side chains from BAK1LRR and flg22 are shown in purple and yellow, respectively. (**B**) Gly^{18} is required for the flg22-induced FLS2LRR-BAK1LRR interaction but not for FLS2 binding in vitro and in null *fls2* mutant mesophyll protoplasts. The assays were performed as described in Fig. 3B. (**C**) The Flg22 G18A mutation has little effect on MPK phosphorylation in mesophyll protoplasts. The assays were performed as described in Fig. 2D. (**D**) Gly^{18} is required for flg22-induced FLS2-BAK1 interaction and the complex activation in seedlings. The assays were performed as described in Fig. 3D. GFP, green fluorescent protein. (**E**) The flg22 G18A mutation modestly affects generation of ROS in planta. WT *Arabidopsis* leaves were treated with water, 100 nM flg22, or 100 nM flg22 G18A.

interaction is further stabilized by two hydrogen bonds formed between Flg22 Leu^{19} and BAK1 Thr^{52} and Val^{54}. Limited by space, any other amino acids at flg22 Gly^{18} would generate steric clashes with the BAK1 loop and consequently attenuate their interaction. Supporting this hypothesis, the mutant peptides flg22 G18A and flg22 G18Y, although they had a comparable FLS2LRR binding activity with the wild-type peptide, exhibited a compromised and no activity of inducing FLS2LRR-BAK1LRR interaction, respectively, in the GST precipitation and Co-IP assay in protoplasts (Fig. 4B and fig. S7B). The mutant peptide flg22 G18A seemed to activate MPKs as efficiently as the wild-type flg22 (Fig. 4C), although it failed to induce an interaction and activation between FLS2 and BAK1 (Fig. 4D). Nevertheless, the generation of reactive oxygen species (ROS) in *Arabidopsis* wild-type Col-0 leaves induced by flg22 G18A and flg22 G18Y was modestly and strongly reduced, respectively (Fig. 4E and fig. S12). The phenotypes generated by the mutations of flg22G^{18} are reminiscent of the *bik1* mutant that is substantially compromised in PAMP-induced resistance but not the flg22-induced MPK activation (*26*), indicating that downstream signaling is differentially affected by perturbations to the receptor complex. An flg22 mutant lacking the C-terminal two residues acts antagonistically with the wild-type peptide (*3*, *23*). This deletion, although not disrupting interaction with FLS2LRR (Fig. 4B and fig. S7), exposes a free carboxylic acid that may perturb the flg22 Gly^{18}–mediated FLS2LRR-BAK1LRR interaction.

As observed for the TLR heterodimers (*24*), the flg22-induced FLS2-BAK1 complex does not seem to be homo-oligomeric for its activation. Ligand-induced homodimerization has been demonstrated in chitin elicitor receptor kinase 1 activation (*27*). Thus, ligand-induced homo- or heterodimerization appears to be a common mechanism of plant receptor kinases and TLRs (*24*) for signaling. TLR4 and its co-receptor, MD-2, homodimerize after lipopolysaccharide binding (*28*), presumably because of the lack of an intracellular signaling domain in MD-2. Similarly, homodimerization or oligomerization could be important for activation of those receptor kinases that form ligand-induced heteromers with receptor-like proteins lacking an intracellular kinase domain.

The sequential recognition of flg22 by FLS2 and BAK1 is required to form a signaling-active complex (Figs. 2 to 4), indicating that BAK1 acts as a co-receptor with FLS2. One feature of the mammalian co-receptors is their promiscuity in ligand binding (*29*). This may also hold true for BAK1 as a co-receptor, because it forms ligand-dependent heteromers with several RKs (*13*, *14*). Indeed, a recent study showed that SERK1 and most likely BAK1 are co-receptors with BRI1 (*30*). The two interfaces between FLS2LRR and BAK1LRR seems collaborative, because mutations in either of them led to a great reduction or loss of FLS2-BAK1 interaction (Figs. 3 and 4). The direct FLS2LRR-BAK1LRR interface could be responsible for formation of the flg22-independent FLS2-BAK1 complex detected in some studies (*9*, *13*, *15*), but it remains possible that the interface is induced by BAK1 recognition of the FLS2-bound flg22. Future studies differentiating the two possibilities will help unravel the mechanism of flg22-induced FLS2-BAK1 activation.

References and Notes

1. T. Boller, G. Felix, *Annu. Rev. Plant Biol.* **60**, 379–406 (2009).
2. C. Zipfel *et al.*, *Nature* **428**, 764–767 (2004).
3. G. Felix, J. D. Duran, S. Volko, T. Boller, *Plant J.* **18**, 265–276 (1999).
4. L. Gómez-Gómez, T. Boller, *Mol. Cell* **5**, 1003–1011 (2000).
5. T. Meindl, T. Boller, G. Felix, *Plant Cell* **12**, 1783–1794 (2000).
6. Z. Bauer, L. Gómez-Gómez, T. Boller, G. Felix, *J. Biol. Chem.* **276**, 45669–45676 (2001).
7. D. Chinchilla, Z. Bauer, M. Regenass, T. Boller, G. Felix, *Plant Cell* **18**, 465–476 (2006).
8. D. Chinchilla *et al.*, *Nature* **448**, 497–500 (2007).
9. B. Schulze *et al.*, *J. Biol. Chem.* **285**, 9444–9451 (2010).
10. K. H. Nam, J. Li, *Cell* **110**, 203–212 (2002).
11. J. Li *et al.*, *Cell* **110**, 213–222 (2002).
12. V. Hecht *et al.*, *Plant Physiol.* **127**, 803–816 (2001).
13. M. Roux *et al.*, *Plant Cell* **23**, 2440–2455 (2011).
14. A. Heese *et al.*, *Proc. Natl. Acad. Sci. U.S.A.* **104**, 12217–12222 (2007).
15. B. Schwessinger *et al.*, *PLOS Genet.* **7**, e1002046 (2011).
16. D. Lu *et al.*, *Proc. Natl. Acad. Sci. U.S.A.* **107**, 496–501 (2010).
17. J. Zhang *et al.*, *Cell Host Microbe* **7**, 290–301 (2010).
18. W. Sun *et al.*, *Plant Cell* **24**, 1096–1113 (2012).
19. S. I. Yoon *et al.*, *Science* **335**, 859–864 (2012).
20. J. She *et al.*, *Nature* **474**, 472–476 (2011).
21. M. Hothorn *et al.*, *Nature* **474**, 467–471 (2011).
22. F. M. Dunning, W. Sun, K. L. Jansen, L. Helft, A. F. Bent, *Plant Cell* **19**, 3297–3313 (2007).
23. K. Mueller *et al.*, *Plant Cell* **24**, 2213–2224 (2012).
24. D. H. Song, J. O. Lee, *Immunol. Rev.* **250**, 216–229 (2012).
25. X. Tan *et al.*, *Nature* **446**, 640–645 (2007).
26. F. Feng *et al.*, *Nature* **485**, 114–118 (2012).
27. T. Liu *et al.*, *Science* **336**, 1160–1164 (2012).
28. B. S. Park *et al.*, *Nature* **458**, 1191–1195 (2009).
29. K. Mythreye, G. C. Blobe, *Cell. Signal.* **21**, 1548–1558 (2009).
30. J. Santiago, C. Henzler, M. Hothorn, *Science* **341**, 889–892 (2013); 10.1126/science.1242468.

Acknowledgments: We thank S. Huang and J. He at Shanghai Synchrotron Radiation Facility (SSRF) for assistance with data collection. This research was funded by State Key Program of National Natural Science of China (31130063) and the National Outstanding Young Scholar Science Foundation of China (31025008) to J.C.; Chinese Natural Science Foundation (31230007) and Chinese Ministry of Science and Technology (2011CB100700) to J.-M.Z.; and the Gatsby Charitable Foundation and the European Research Council to C.Z. A.P.M. is supported by a postdoctoral fellowship from the Federation of European Biochemical Societies. The coordinates and structural factors for FLS2LRR-flg22-BAK1LRR and FLS2ΔLRR2-6 have been deposited in Protein Data Bank with accession codes 4MN8 and 4MNA, respectively.

Supplementary Materials

www.sciencemag.org/content/342/6158/624/suppl/DC1
Materials and Methods
Figs. S1 to S12
Table S1
References (*31*–*38*)

26 July 2013; accepted 30 September 2013
Published online 10 October 2013;
10.1126/science.1243825

Regulation of Temperature-Responsive Flowering by MADS-Box Transcription Factor Repressors

Jeong Hwan Lee,[1] Hak-Seung Ryu,[1] Kyung Sook Chung,[1] David Posé,[2]* Soonkap Kim,[1] Markus Schmid,[2] Ji Hoon Ahn[1]†

Changes in ambient temperature affect flowering time in plants; understanding this phenomenon will be crucial for buffering agricultural systems from the effects of climate change. Here, we show that levels of *FLM-β*, an alternatively spliced form of the flowering repressor *FLOWERING LOCUS M*, increase at lower temperatures, repressing flowering. FLM-β interacts with SHORT VEGETATIVE PHASE (SVP); SVP is degraded at high temperatures, reducing the abundance of the SVP–FLM-β repressor complex and, thus, allowing the plant to flower. The *svp* and *flm* mutants show temperature-insensitive flowering in different temperature ranges. Control of SVP–FLM-β repressor complex abundance via transcriptional and splicing regulation of *FLM* and posttranslational regulation of SVP protein stability provides an efficient, rapid mechanism for plants to respond to ambient temperature changes.

For plants, successful reproduction requires careful timing of flowering to match pollinator availability and growing-season temperature restrictions. Multiple environmental factors, including day length and temperature, affect this crucial change from vegetative to reproductive growth (*1*–*3*). Various components regulate flowering in response to extremes in temperature such as cold (vernalization) or heat stress (*4*, *5*). Small changes in ambient temperature also affect flowering time (*6*–*8*), with colder temperatures generally delaying flowering. However, our understanding of ambient temperature–responsive flowering remains limited. Because day length and temperature